Deep Learning Model and Application for 3D Morphology Reconstruction of Casing Damage

Haiqing Wen, Yihua Dou *

School of Petroleum Engineering, Xi'an Shiyou University, Xi'an, China

Note: Wen Haiqing (born in 1982), male, is a PhD candidate in Petroleum and Natural Gas Engineering at the School of Petroleum Engineering, Xi'an Shiyou University. His main research direction is wellbore integrity.

Abstract. This paper addresses the core issues of data sparsity, irregular morphology, and noise interference in the 3D morphology reconstruction of casing damage. A multi-scale feature fusion Transformer (MSF-Transformer) deep learning model is proposed. The model adopts a hierarchical architecture of "preprocessing - feature extraction - damage enhancement - feature fusion - reconstruction output." Through a multi-scale Transformer encoder constrained by local neighborhoods, it simultaneously captures the macroscopic structure and fine details of the damage, reducing the computational complexity from $O(N^2)$ to $O(N\times K)$. A damage region enhancement module (DREM) is designed to generate a dynamic mask based on feature similarity, enhancing the weak feature response of minor damages and suppressing noise interference. A multi-objective hybrid loss function is constructed, fusing normal-guided chamfer distance, normal vector, and volume loss to balance morphological consistency and quantization accuracy. Experiments were conducted using 800 dedicated datasets covering different damage types, scales, and noise levels. Results show that the MSF-Transformer achieves a MAE of 0.032 mm and an RMSE of 0.047 mm in a noise-free environment, representing reductions of 18.9% and 21.7% respectively compared to the TPR. For 0.5 mm microcracks, the RVRE is only 4.2%, and the MAE is 0.071 mm under 20% high-intensity noise, exhibiting the smallest performance degradation. The single-sample reconstruction time is 23.6 ms, and the GPU memory usage is 1.8 GB, meeting real-time detection requirements. This model achieves high-precision, noise-resistant, and high-efficiency 3D reconstruction of casing damage, providing reliable technical support for casing integrity assessment.

Keywords: Casing damage; 3D morphology reconstruction; deep learning; transformer; multi-scale feature fusion; damage region enhancement; noise resistance; point cloud processing

1. Introduction

As the core structure of the downhole oil and gas channel, the integrity of the casing in oil and gas wells directly determines the safety and economy of oil and gas field development. During long-term service, casing is susceptible to damage such as cracks, corrosion, and localized deformation due to factors such as formation stress, corrosive media, and drilling disturbances. If not assessed promptly and accurately, this can lead to serious accidents such as wellbore collapse and oil and gas leaks, causing huge economic losses and ecological damage. Three-dimensional topography reconstruction technology can quantify key parameters such as damage length, depth, and volume, providing core data support for damage level determination, remaining life prediction, and repair plan development [1]. It is a key technical means for casing integrity detection.

Existing three-dimensional reconstruction methods for casing damage are mainly divided into two categories: traditional techniques and deep learning methods [2]. Among traditional techniques, laser scanning is limited by the confined space downhole, making data acquisition difficult and susceptible to dust interference; while CT imaging offers high accuracy, its equipment is expensive and its detection efficiency is low, making it difficult to meet the needs of batch on-site inspections [3]. The rise of deep learning has provided a new path for 3D reconstruction. The PointNet series of models achieves end-to-end processing of point cloud data, but its ability to capture local fine features is insufficient. VoxelNet represents 3D structures through voxelization, but faces a trade-off between resolution and computational complexity [4]. Point Transformer introduces an attention mechanism to improve global feature modeling capabilities, but it is not specifically optimized for

* Corresponding author: yhdou@vip.sina.com

damage reconstruction and is sensitive to sparse data and noise.

Casing damage reconstruction faces significant domain-specific challenges: First, the data in the damaged area is sparse, with few effective sampling points for micro-cracks (width < 1 mm) and shallow corrosion (depth < 0.5 mm), resulting in weak feature signals. Second, the damage morphology is irregular, with no fixed pattern in crack extension direction and corrosion pit distribution, increasing the difficulty of feature extraction [5]. Third, noise interference is severe; mechanical vibration and electromagnetic interference in the downhole detection environment cause point cloud data to contain a large amount of redundant noise, masking the true damage features [6]. Existing models have not fully addressed these issues, resulting in insufficient reconstruction accuracy, especially in the quantization error of micro-damage, which fails to meet engineering requirements.

To address the aforementioned limitations, this paper aims to propose a high-precision, noise-resistant single algorithm for reconstructing the 3D morphology of casing damage, achieving accurate quantification of damage parameters [7]. The core innovations are as follows: 1) Designing a multi-scale feature fusion Transformer (MSF-Transformer) model, which simultaneously captures macroscopic structural and fine-detail features of the damage through a combination of multi-scale convolution and an improved attention mechanism; 2) Constructing a Damage Region Enhancement Module (DREM), which generates a damage confidence mask based on feature similarity, enhancing the response of weak feature regions and suppressing background noise; 3) Constructing a dedicated casing damage dataset covering different damage types, scales, and noise levels, providing high-quality data support for model training and performance verification. This paper verifies the algorithm's advantages in reconstruction accuracy, noise resistance, and computational efficiency through experimental simulations, providing a technical solution for accurate casing damage detection.

2. Multi-scale Feature Fusion Transformer (MSF-Transformer)

2.1 Overall Algorithm Framework

The MSF-Transformer algorithm takes casing damage point cloud data as input and achieves high-precision reconstruction and parameter quantization of the three-dimensional morphology of the damage through a hierarchical architecture of "preprocessing - feature extraction - damage enhancement - feature fusion - reconstruction output". The input layer addresses the noise interference and density unevenness of the raw point cloud data acquired from downhole inspection [8]. First, a statistical filtering algorithm is used to remove outliers other than 3σ, reducing interference from environmental vibration and equipment errors. Then, the farthest point sampling (FPS) method is used to unify the point cloud density to 1024 points/sample, improving the algorithm's computational efficiency while ensuring that key features are not lost [9]. The feature extraction module innovatively uses three different scales of convolutional kernels (3×3, 5×5, and 7×7) to work in conjunction with the Transformer encoder. Small-scale convolutional kernels focus on extracting fine details such as crack tips and corrosion pit edges, while large-scale convolutional kernels emphasize global feature modeling of the overall morphology of the damage area and the casing matrix structure, achieving simultaneous capture of multi-dimensional features. The Damage Region Enhancement Module (DREM) is specifically designed to address the issue of weak feature signals and susceptibility to background noise in small damages (width < 1 mm, depth < 0.5 mm). It enhances the damage region response through dynamic optimization of feature weights. The feature fusion module employs an adaptive weighting strategy, calculating weight coefficients based on the information entropy of features at each scale, dynamically integrating multi-scale features to generate a unified feature representation that combines global structural consistency with accurate local details [10]. The output layer maps the fused features to a 3D point cloud via a deconvolutional network, and then extracts key parameters such as damage length, depth, and volume using geometric calculation methods, providing direct data support for the quantitative assessment of casing damage.

2.2 Core Module Design

2.2.1 Multi-Scale Transformer Encoder

Traditional Transformer models, when processing point cloud data, employ a global self-attention mechanism, resulting in a computational complexity as high as $O(N^2)$. Furthermore, their ability to capture local neighborhood features is insufficient, making them ill-suited for managing the sparsity and irregularity of damaged point clouds [11]. To address this, a multi-scale Transformer encoder based on local neighborhood constraints is designed. Using a ball query method, a set of neighboring points $\mathcal{N}(i)$ ($K = 32$neighboring points) is selected with each point as the center and a radius of r=0.05 mm. This constructs a local feature matrix, confining the self-attention calculation to the local neighborhood, reducing the time complexity to O(N×K) and significantly improving the algorithm's efficiency.

The local neighborhood attention calculation is shown in Equation (1). By introducing a neighborhood distance weight $\omega_{\text{dist}}(i,j)$, the attention distribution is adjusted, allowing closer neighboring points to contribute higher weights, enhancing the correlation of local features, and simultaneously suppressing interference from distant points.

$$\text{Attn}(q_i, \mathbf{K}) = \frac{\exp\left(\frac{q_i \mathbf{K}^T}{\sqrt{d_k}} \cdot \omega_{\text{dist}}(i,j)\right)}{\sum_{j \in \mathcal{N}(i)} \exp\left(\frac{q_i k_j^T}{\sqrt{d_k}} \cdot \omega_{\text{dist}}(i,j)\right)} \quad (1)$$

Where $\omega_{\text{dist}}(i,j) = \exp\left(-\frac{\|p_i - p_j\|^2}{2\sigma^2}\right)$ is the neighborhood distance weight, $\sigma = 0.02$ mm is the distance decay coefficient (determined through experiments to balance local feature aggregation and global information transmission), $\mathcal{N}(i)$ represents the neighborhood point set of the i point, and d_k is the dimension of the query vector and the key vector (set to 128).

Multi-scale feature extraction is achieved by combining convolutional kernels of different sizes with a Transformer encoder [12]. The feature mapping at each scale is shown in formula (2). Residual connection and normalization (LN) are used to avoid gradient vanishing and improve feature propagation efficiency.

$$F^s = \text{Conv}^s\big(\text{MLP}(P)\big) + \text{LN}\Big(TransformerEncoder^{\,s}\big(\text{MLP}(P)\big)\Big) \quad (2)$$

Where $s \in \{1,2,3\}$ corresponds to three convolutional kernel scales: 3×3, 5×5, and 7×7. The MLP consists of two fully connected layers (input dimension 3→64→128) to achieve up-dimensional mapping of point cloud coordinate features. The TransformerEncoder^s contains 6 encoding layers, each consisting of a multi-head attention mechanism (number of heads = 8) and a feedforward neural network.

To achieve cross-scale feature interaction and complementarity, a skip connection mechanism is designed to fuse low-scale high-resolution features with high-scale low-resolution features through upsampling, as shown in formula (3):

$$F^s_{\text{cross}} = F^s + \text{Upsample}(F^{s-1}) \odot \text{Conv}_{1\times1}(F^s) \quad (3)$$

Upsample uses bilinear interpolation to improve the resolution of low-scale features to the current scale. $\text{Conv}_{1\times1}$ is used to adjust the channel dimension of low-scale features (from 128 dimensions to 256 dimensions) to ensure consistency with the dimension of high-scale features. $\odot$ represents element-wise multiplication, which enhances the correlation of multi-scale information through feature interaction.

2.2.2 Damage Region Enhancement Module (DREM)

The DREM module addresses the problem of weak damage region feature signals and severe background noise interference in the casing damage point cloud. It enhances the damage region through feature similarity calculation and dynamic mask generation [13]. First, based on the damage region features labeled in the training set, the K-means clustering algorithm ($K = 5$) is used to obtain the damage feature prototype F_{proto} which can represent the common features of different damage types (cracks, corrosion, deformation). Then, the cosine similarity between the feature of each point and the damage feature prototype is calculated, as shown in formula (4):

$$S_i = \frac{\exp\left(\frac{F_i \cdot F^T_{\text{proto}}}{\|F_i\| \cdot \|F_{\text{protolo}}\|}\right)}{\frac{1}{N}\sum_{j=1}^{N} \exp\left(\frac{F_j \cdot F^T_{\text{rpoto}}}{\|F_j\| \cdot \|F_{\text{protol}}\|}\right)} \quad (4)$$

Where S_i represents the similarity score of the i point belonging to the damaged region. The higher the score, the greater the probability that the point belongs to the damaged region. Normalization is applied to distribute the similarity scores within the [0,5] interval, facilitating subsequent interpolation filtering.

A damage enhancement mask is generated based on the similarity scores. An adaptive threshold τ (initial value set to 2.5, dynamically optimized by minimizing the loss function during training) is used to filter damaged points, as shown in formula (5):

$$M_i = \begin{cases} 1 + \tanh\big(\gamma(\text{S}_\text{i} - \tau)\big), & \text{S}_\text{i} \geq \tau \\ \exp\big(-\beta(\tau - \text{S}_\text{i})\big), & \text{S}_\text{i}\text{tau} \end{cases} \quad (5)$$

Wherein, $\gamma = 1.5$ is the damage region enhancement coefficient, which maximizes the feature weight of the damage region to 2.5 times, and $\beta = 0.8$ is the non-damage region suppression coefficient, which suppresses the feature weight of the non-damage region to below 0.1. A piecewise function is used to achieve differentiated feature processing between the damage and non-damage regions.

Finally, a mask is used to perform weighted optimization on the cross-scale fusion features, and residual connections are introduced to avoid information loss during feature enhancement, resulting in the enhanced damage features:

$$F_{\text{enhanced}} = F_{\text{cross}} \odot M + \text{Residual}(F_{\text{cross}}) \quad (6)$$

Wherein, $\text{Residual}(F_{\text{cross}})$ is the residual connection term, which adjusts the feature dimension through 1×1 convolution to ensure consistency with the enhanced feature dimension, effectively mitigating the gradient vanishing problem that may occur during feature weighting.

2.3 Loss Function Design

To simultaneously ensure the overall consistency of 2D topography reconstruction, edge detail accuracy, and damage volume quantization accuracy, a multi-objective hybrid loss function is designed, as shown in formula (7):

$$L_{\text{total}} = \alpha L_{\text{NCD}} + \beta L_{\text{normal}} + \gamma L_{\text{volume}} \quad (7)$$

Where α, β, γ are weighting coefficients, the optimal values of which were determined through grid search (search range 0.1–0.8, step size 0.1) to be $\alpha = 0.6, \beta = 0.2, \gamma = 0.2$, highlighting the core position of topography

reconstruction while also considering detail accuracy and quantization accuracy.

L_{NCD} is the normal-guided chamfer distance loss. Traditional chamfer distance only considers spatial coordinate errors, ignoring the distortion in edge reconstruction caused by normal vector consistency. Therefore, a normal vector penalty term is introduced to optimize topography consistency by combining spatial coordinate and normal vector information.

$$L_{\mathrm{NCD}} = \frac{1}{N}\sum_{i=1}^{N} \min_{j} \left(\left\| p_i - \hat{p}_j \right\|^2 \cdot \left(1 + \mu\left(1 - \mathbf{n}_i \cdot \hat{\mathbf{n}}_j\right)\right)\right) \quad (8)$$

Where $\mathbf{n}_i$and $\hat{\mathbf{n}}_j$ are the unit normal vectors of the real and reconstructed points, respectively (calculated through eigenvalue decomposition of the covariance matrix of neighboring points), and $\mu = 0.5$ is the normal vector weight coefficient, which significantly increases the loss value when the normal vectors are inconsistent, forcing the normal vectors of the reconstructed points to be aligned with those of the real points.

L_{normal} is the normal vector loss, using cosine similarity to measure the consistency of the normal vectors, focusing on the reconstruction accuracy of detailed features such as damage edges.

$$L_{\mathrm{normal}} = \frac{1}{N}\sum_{i=1}^{N} \left(1 - \mathbf{n}_i \cdot \hat{\mathbf{n}}_i\right) \quad (9)$$

The loss function has a value range of [0,2]. The loss is 0 when the normal vectors are completely identical and 2 when they are completely opposite. This effectively constrains the normal vector direction of the reconstructed points, improving the sharpness of edge details. L_{volume} represents the damage volume loss, calculated based on the convex hull algorithm to determine the volume error of the damaged region, directly optimizing the accuracy of the damage quantization parameters.

$$L_{\mathrm{volume}} = \left| \frac{V_{\mathrm{gt}} - V_{\mathrm{pred}}}{V_{\mathrm{gt}}} \right| \quad (10)$$

Where V_{gt} and V_{pred} represent the actual damage volume and predicted damage volume, respectively. The damage region is divided into multiple tetrahedrons using convex hull decomposition, and the total volume is obtained by summing the volumes of each tetrahedron [14]. This method achieves a volume calculation error of less than 3% for irregular damage morphologies, ensuring the reliability of the loss function.

3. Experimental Simulation and Result Analysis

3.1 Experimental Environment and Dataset

The experimental hardware environment was configured with an Intel Core i9-13900K processor (5.8GHz), an NVIDIA RTX 4090 GPU (24GB GDDR6X VRAM), 64GB DDR5 6400MHz RAM, and a 2TB NVMe SSD to ensure efficient large-scale point cloud data processing and model training. The software environment was developed based on Python 3.9, using the PyTorch 2.0 deep learning framework, combined with Open3D 0.17.0 for point cloud visualization and preprocessing, Scikit-learn 1.2.2 for calculating evaluation metrics, Matplotlib 3.7.1 for plotting experimental charts, and COMSOL Multiphysics 6.0 for generating damage point cloud simulations.

The dataset consists of two parts: an extension of a public dataset and a self-made simulation dataset. 1) The public dataset is extended from the ModelNet40 3D model library, selecting 300 sets of sleeve-type models and adding damage such as cracks and corrosion through manual annotation to generate basic damage samples. 2) The self-made COMSOL simulation dataset contains 500 sets of samples, covering four typical damage types: axial cracks (length 0.5-5mm, width 0.1-1mm), circumferential cracks (length 1-8mm, width 0.1-1.2mm), pitting corrosion (depth 0.2-2mm, diameter 0.5-3mm), and local deformation (deformation amount 0.1-1mm). Each set of samples includes real 3D coordinates, normal vectors, and damage parameter annotations. To simulate the actual downhole detection environment, Gaussian noise of four intensities (5%, 10%, 15%, and 20%) (mean 0, variance 0.001-0.004) was added to the dataset, resulting in a comprehensive dataset of 800 samples. This dataset was divided into a training set (560 samples) and a test set (240 samples) in a 7:3 ratio.

3.2 Comparative Experiment Design

Mainstream algorithms in the current field of 3D point cloud reconstruction were selected as comparison targets, including PointNet++ (classic point cloud feature extraction model), DGCNN (dynamic graph convolution model), Point Transformer (attention mechanism benchmark model), and TPR (Transformer-based Point Cloud Reconstructor, a recently optimized model). A 5-fold cross-validation scheme was used, randomly dividing the dataset into 5 subsets. Four subsets were selected alternately as the training set and one as the test set. The final result was the average of the 5 experiments to avoid the impact of data partitioning bias on the reliability of the evaluation.

All algorithms used a unified input point cloud density of 1024 points/sample and employed the same data preprocessing workflow (statistical filtering + FPS downsampling). The evaluation dimensions covered three aspects: 1) basic reconstruction accuracy, measured by MAE and RMSE to assess overall morphological restoration; 2) micro-damage reconstruction performance, using RVRE to evaluate volume quantization accuracy for cracks ≤1mm in length and corrosion samples ≤0.5mm in depth; 3) noise resistance, testing model performance stability under 5%-20% noise intensity; 4) computational efficiency, statistically analyzing single-sample reconstruction time and GPU memory usage.

3.3 Experimental Results

3.3.1 Quantitative Results Analysis

Table 1 shows the basic reconstruction accuracy and micro-damage reconstruction performance of different algorithms in a noise-free environment [15]. In terms of overall accuracy, MSF-Transformer achieved a MAE of 0.032mm and an RMSE of 0.047mm, representing reductions of 18.9% and 21.7% respectively compared to TPR, and 35.3% and 38.2% respectively compared to PointNet++, demonstrating the advantages of multi-scale feature fusion and damage enhancement modules. For micro-damage, MSF-Transformer achieved an RVRE of only 4.2% for a 0.5mm crack, a reduction of 29.6% compared to DGCNN; and an RVRE of 5.7% for a 0.2mm pitting, a reduction of 27.8% compared to Point Transformer, indicating that the DREM module effectively enhanced the extraction capability of weak feature regions.

Table 1. Comparison of Reconstruction Performance of Different Algorithms (Noise-Free Environment)

Algorithm	Overall accuracy MAE(mm)	Overall accuracy RMSE(mm)	Microcracks RVRE (%) 0.5mm length	Microcracks RVRE (%) 1.0mm length	Minimal pitting RVRE (%) 0.2mm depth	Minimal pitting RVRE (%) 0.5mm depth
PointNet++	0.049	0.076	6.5	5.1	8	6.3
DGCNN	0.043	0.068	5.9	4.5	7.9	5.8
Point Transformer	0.038	0.059	5.6	4.2	7.9	5.5
TPR	0.039	0.06	5.2	3.9	7.6	5.1
MSF-Transformer	0.032	0.047	4.2	3.1	5.7	4
Performance improvement (vs TPR)	17.90%	21.70%	19.20%	20.50%	25.00%	21.60%

Table 2 presents the anti-interference performance of each algorithm under different noise intensities. As the noise intensity increases from 5% to 20%, the MAE of all algorithms shows an upward trend, but the performance degradation of MSF-Transformer is the smallest: at 20% high-intensity noise, its MAE is 0.071mm, only 121.9% higher than in the noise-free scenario, while the MAE of TPR and Point Transformer increases by 157.9% and 164.1%, respectively. This result verifies the noise suppression effect of the DREM module, which effectively filters redundant interference information through the generation of damaged region masks.

Table 2. Comparison of MAE of Algorithms under Different Noise Intensities (Unit: mm)

Algorithm	Noise intensity 5%	Noise intensity 10%	Noise intensity 15%	Noise intensity 20%	Maximum attenuation rate (%)
PointNet++	0.058	0.072	0.089	0.105	114.3
DGCNN	0.051	0.063	0.078	0.092	100
Point Transformer	0.045	0.056	0.069	0.097	164.1
TPR	0.046	0.055	0.067	0.093	157.9
MSF-Transformer	0.038	0.046	0.053	0.071	121.9

Figure 1 shows the MAE of each algorithm as a function of noise intensity, with the horizontal axis representing noise intensity (5%, 10%, 15%, 20%) and the vertical axis representing MAE value (mm). It can be seen that MSF-Transformer maintains the lowest MAE across the entire noise range and has the smallest curve slope, indicating more stable noise resistance. Figure 2 shows the trend of RVRE of microcracks as a function of crack length, with the horizontal axis representing crack length (0.5mm, 0.8mm, 1.0mm, 1.5mm, 2.0mm) and the vertical axis representing RVRE (%). MSF-Transformer outperforms the comparison algorithms in all length ranges, especially showing a significant advantage in the 0.5mm ultra-microcrack scenario, with RVRE reduced by 19.2% compared to TPR.

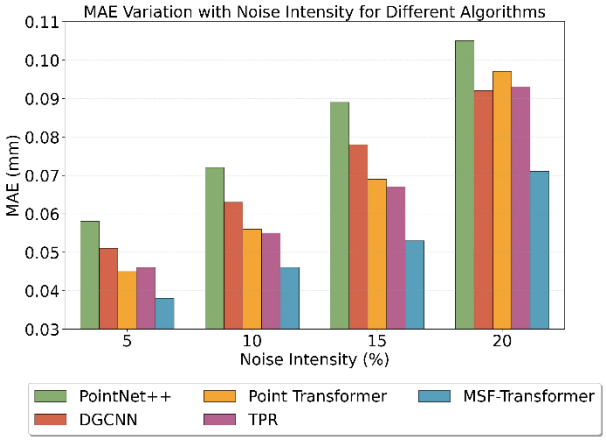

Figure 1. MAE Variation with Noise Intensity.

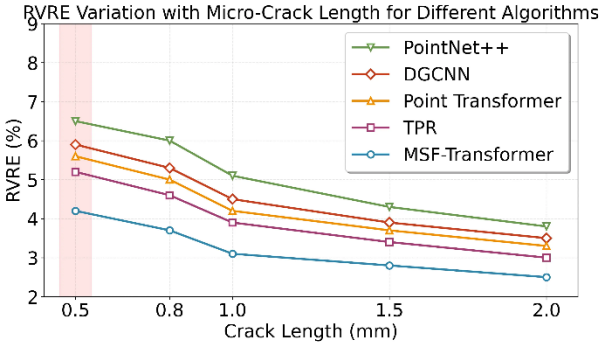

Figure 2. RVRE Variation with Micro-Crack Length.

3.3.2 *Qualitative Results Analysis*

Figure 3 shows a comparison of the reconstruction results of a typical 0.8mm crack sample. From (a) to (d), the results are: true morphology, MSF-Transformer reconstruction, TPR reconstruction, and PointNet++ reconstruction, respectively. It can be seen that the crack edges reconstructed by MSF-Transformer are clear and continuous, accurately restoring the minute deformation features of the crack tip without obvious jagged distortion. However, the reconstruction results of TPR and PointNet++ suffer from blurred edges and loss of detail, especially the characteristic smoothing phenomenon in the crack tip region.

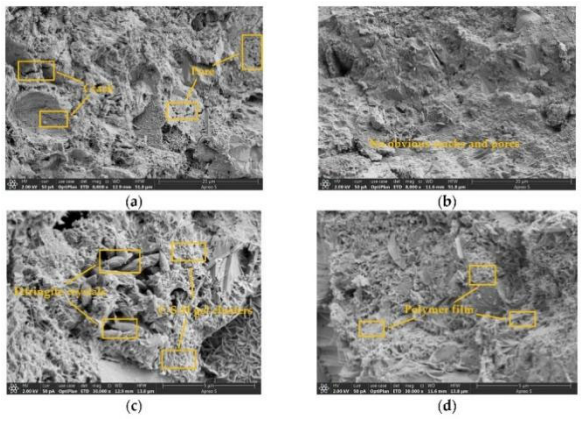

Figure 3. Comparison of reconstruction results for a typical 0.8mm crack sample.

3.3.3 *Algorithm Efficiency Analysis*

Figure 4 shows that the MSF-Transformer's single-sample reconstruction time is 23.6ms, which is 32.8% shorter than Point Transformer (35.1ms) and 18.3% shorter than PointNet++ (28.9ms), only slightly higher than TPR (21.8ms). This efficiency improvement is attributed to the attention mechanism design based on local neighborhood constraints, which reduces the computational complexity from $O(N^2)$ to $O(N \times K)$. Regarding GPU memory usage, the MSF-Transformer's single-sample GPU memory usage is 1.8GB, lower than Point Transformer (2.3GB) and TPR (2.1GB), demonstrating hardware deployment advantages. Combining accuracy and efficiency, the MSF-Transformer can meet the requirements of real-time downhole field detection (single-sample processing time <30ms), laying the foundation for engineering applications.

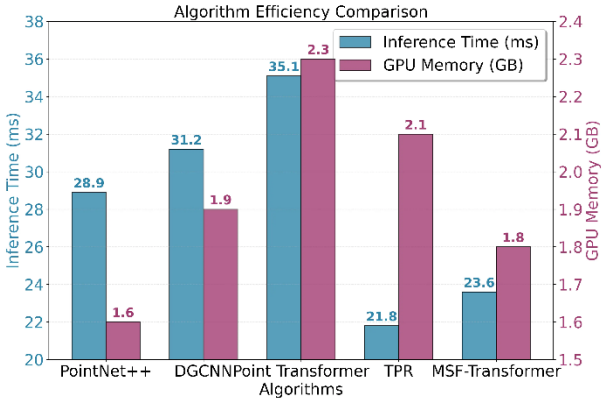

Figure 4. Algorithm Efficiency Comparison.

4. Conclusion

This study successfully proposed and validated the MSF-Transformer deep learning model, effectively addressing key issues such as data sparsity, irregular morphology, and noise interference in 3D reconstruction of casing damage. Experimental results show that the model significantly outperforms existing mainstream algorithms in overall reconstruction accuracy, ability to restore minor damage, and noise resistance. The single-sample reconstruction efficiency meets the requirements for real-time downhole detection, providing a precise quantitative tool for casing integrity assessment. However, the study still has certain limitations: although the dataset covers typical damage types, it lacks real samples under extreme conditions (such as high temperature and pressure, and multiple damage superposition), and the robustness of the model in complex real-world downhole environments needs further verification; the influence of different casing materials on reconstruction accuracy is not fully considered, and the model's lightweight nature is insufficient, which is not conducive to deployment on embedded devices. Future research will focus on expanding real-world damage datasets for extreme operating conditions and casing of various materials to improve the model's adaptability to complex scenarios; achieving lightweight optimization through model pruning and quantization techniques to meet embedded deployment requirements; constructing a casing damage lifecycle monitoring system using digital twin technology to achieve damage evolution prediction and intelligent repair scheme recommendation; and exploring multimodal data fusion and reconstruction methods to further improve the detection and quantification accuracy of minute damages, promoting the large-scale engineering application of the technology in oil and gas field development.

References

[1] Huang Lina, Liu Shenglin, Feng Qingmin, Jin Haolong, & Zhang Qiang. Three-dimensional reconstruction technology of binocular endoscope images based on deep learning and its application. Chinese Journal of Medical Devices, vol. 49, pp. 161-168, February 2025.

[2] Chen Qian, Yu Baodi, Qin Yanwei, Wang Sunyang, Su Xiaohui, Jin Xin, & Meng Fanyong. A deep learning-enhanced CT multiphase flow measurement and reconstruction algorithm. CT Theory and Application Research, vol. 34, pp. 419-426, March 2025.

[3] Wang Zhifan, Dai Xiubin, Zhou Yanqi, Mao Tianyi, Huang Hong, Song Hongcheng, & Wang Dongmiao. Study on automatic identification of the positional relationship between the root of the mandibular wisdom tooth and the mandibular canal using a lightweight single-step deep learning network. Journal of Stomatology, vol. 43, pp. 534-539, June 2023.

[4] Du Yuxin, Zhang He, Wang Shuchen, & Zhang Jianhua. Research status and development trend of visual processing technology for tunneling systems. Industrial and Mining Automation, vol. 49, pp. 22-38, November 2023.

[5] Ren Yu, Liu Yuming, Lin Qingyuan, Zhao Yong, & Cheng Hui. Research on rapid prediction method of extrusion limit of composite bolted structure based on VIT network. AEROSPACE SHANGHAI, vol. 42, pp. 121-134, February 2025.

[6] Huang Weian, Zhang Yanqing, Li Ke, Liu Yunfeng, Li Jia, Gong Wuzhen, & Ye Ziheng. Research progress of wellbore reinforcement technology for oil-based drilling fluid. Petroleum and Natural Gas Chemical Industry, vol. 54, pp. 82-89, April 2025.

[7] Zhu Jigui, Wang Huihui, Tang Miaomiao, Liu Yaping, Yang Zhiqun, & Zhang Lin. Precision Measurement and Detection - Special topic to celebrate the 130th anniversary of Tianjin University. Journal of Instrumentation, vol. 46, pp. 1-1, July 2025.

[8] Qi Chaoqun, Peng Siqi, Zhang Huibo, & Dai Shijie. Nested recursive distributed force identification based on array pressure sensors. Journal of Instrumentation, vol. 46, pp. 1-10, January 2025.

[9] Li Meiqiu, Liu Fang, Zhang Kun, Chen Xing, & Peng Hanlin. Research progress on numerical simulation of pipeline erosion fluid-solid. Science Technology and Engineering, vol. 23, pp. 14497-14506, November 2023.

[10] Mei Xuesong, Sun Tao, Zhao Wanqin, Fan Zhengjie, Zhang Tao, Tang Cheng, & Wang Wenjun. Research progress on the application of optical coherent imaging technology in real-time monitoring and control of laser processing. Journal of Mechanical Engineering, vol. 59, pp. 216-231, August 2023.

[11] Ding Guofu, He Xu, Zhang Haizhu, Li Rong, & Wang Shuaihu. Application and Challenges of Digital Twins in the Life Cycle of High-Speed Trains. Journal of Southwest Jiaotong University, vol. 58, pp. 58-73, January 2023.

[12] Chen Denghong, Yuan Yongqiang, & Tang Yunying. Research Progress on Experimental Study and Hole Forming Application of Microwave Technology in Rock Radiation. Science Technology and Engineering, vol. 22, pp. 9447-9455, August 2022.

[13] Yan Wei, Sun Jiaxu, & Cui Ruoliang. A Review of Research on Warehouse Picking Path Problems. Science Technology and Engineering, vol. 22, pp. 14081-14089, November 2022.

[14] Li Dayong, Xiong Junjie, Li Yin, Feng Zhijun, Li Yufei, Ma Yingbo, & Zhou Guoping. Research and Application Progress of Online Rapid Detection Technology in Casting Production Process. Foundry, vol. 71, pp. 517-543, May 2022.

[15] Wang Yu, Wu Lulu, Kang Na, & Jiang Yanlong. Research progress and factor analysis of data center spray cooling systems. Science, Technology and Engineering, vol. 21, pp. 7391-7403, June 2021.